

Mind blanking is associated with a rigid spatio-temporal profile in typical wakefulness

Sepehr Mortaheb^{1,2}, Manousos A. Klados³, Laurens Van Calster^{4,5}, Paradeisisos Alexandros Boulakis¹, Kleio Georgoula¹, Steve Majerus^{2,4,5}, and Athena Demertz^{1,2,4,5*}

¹Physiology of Cognition Lab, GIGA-Consciousness, University of Liège, Liège, Belgium

²Fund for Scientific Research FNRS, Brussels, Belgium

³Department of Psychology, CITY College, University of York Europe Campus, Thessaloniki, Greece

⁴Psychology and Neuroscience of Cognition Research Unit, University of Liège, Liège, Belgium

⁵GIGA-Cyclotron Research Center In Vivo Imaging, University of Liège, Liège, Belgium

*Corresponding Author: Athena Demertz

Email: a.demertz@uliege.be

Address: Physiology of Cognition Lab, GIGA-Consciousness, GIGA Research Institute B43, Avenue de l'Hôpital 11, 4000 Liège, Belgium

1 Abstract

2 Mind-blanking (MB) is the inability to report mental contents, challenging the view of a constantly thought-oriented mind
3 during wakefulness. Using fMRI experience-sampling we show that MB is reported scarcely, fast, and has low transitional
4 dynamics, pointing to its role as a transient mental relay. MB's cerebral profile is linked to an overall positive connectivity
5 pattern, bearing great resemblance to neural configurations observed in local sleeps, possibly reflecting neuronal silencing
6 during wakefulness. We also find less efficient information flow between the default mode (DMN) and other networks before
7 reporting MB. The DMN-salience network segregation was further able to classify MB from other reports in fewer steps,
8 suggestive of an early saliency evaluation of contentless phenomenology along the neurocognitive hierarchy. Collectively,
9 MB's unique neurofunctional profile among thought-oriented reports supports the view of instantaneous mental absences
10 happening during wakefulness, paving the way for more mechanistic investigations of this particular phenomenology during
11 ongoing mentation.

12 1 Introduction

13 During spontaneous thinking we tend to traverse different mental states which recruit the activity of multiple neural systems¹.
14 What is interesting is that, apart from entertaining specific thoughts, there are moments when our minds go nowhere, giving the
15 impression that we are empty of mental content. These phenomenological occurrences are known as content-free awareness² or
16 mind blanking (MB)³. What is the position of MB among other mental states during ongoing thinking, and how does the brain
17 configure to support this empty-mind phenomenology?

18 Behavioral studies indicate that MB happens scarcely during everyday functioning, yet with a considerable frequency. It
19 has been shown, for example, that during focused tasks, MB was reported on average 14.5% of the time whenever subjects
20 were requested to provide a mental evaluation³, and 18% of the time when participants reported MB by self-catching⁴. MB was
21 also observed in the form of attentional lapses, when participants were engaged in task performance⁵⁻⁷. In terms of neural
22 underpinnings, there was evidence for reduced fMRI functional connectivity between the default mode network (DMN) and
23 frontal, visual, and salience networks when participants were instructed to "think of nothing" as compared to "let your mind
24 wander"⁸. MB was also associated with deactivation of Broca's area and parts of the hippocampus, as well as with activation
25 of the anterior cingulate cortex, which was interpreted as reduced inner speech⁹. Decreased functional connectivity in the
26 posterior regions of the DMN and increased connectivity in the dorsal attentional network were also found in an experienced
27 meditator practicing content-minimized awareness². Collectively, these studies indicate that the investigation of MB is rising
28 over the years. Yet, MB so far has been induced, therefore the estimation of its occurrences across time can be biased. Also,
29 MB has been examined in highly-trained individuals, like experienced meditators, therefore limiting the generalizability of its
30 occurrences in typical participants. Finally, the neural substrates associated with MB concern a limited number of brain regions,
31 leaving the whole-brain functional connectome uncharted.

32 The importance of a comprehensive characterization of MB rests on the fact that MB challenges the view of a primarily
33 thought-oriented mind, which traverses stimulus-dependent and stimulus-independent thoughts¹⁰. Mind states which are
34 thought-oriented indeed prevail during wakeful mentation and are characterized by rich spatio-temporal dynamics at the
35 brain level¹¹. Inversely, less complex neural architectures of highly segregated organization and less metastable dynamics are
36 linked to the inability to report subjective experience as seen in sleep¹², anesthetized primates¹³, typical individuals under
37 anesthesia¹⁴, and in vegetative/unresponsive patients¹⁵. Several theoretical models concur that the reason we cannot report
38 in such a segregated state is because the brain is unable to combine divergent signals and distribute them widely so that they
39 become reportable^{16,17}. These theoretical frameworks further hold that the inability to report mental contents can also happen
40 in a brain state with extreme functional integration. In this scenario, an abnormally large number of regions work in synchrony,
41 and, as a result, the brain becomes no longer capable of processing information in a way that leads to reportability, such as
42 during generalized epilepsy¹⁸ and local sleeps¹⁹. As both neural configurations can occur during ongoing mentation¹⁵ and can
43 be linked to the inability to report, the emerging question is which one would support the phenomenology of MB. To date, no
44 empirical evidence favours one possibility over the other.

45 With the aim to delineate the neurofunctional profile of MB, we used fMRI-based experience-sampling in typical individuals²⁰ in order to: a) account for a representative behavioral quantification of pure (no induction) MB occurrences in a dynamic
46 way, b) determine MB's functional connectome at the whole-brain level, and c) estimate the brain's segregative/integrative
47 way whenever reporting MB occurrences.
48

49 Results

50 Data were acquired from 36 typical participants (27 females, 9 males, mean age: 23y±2.9) within a 3T MRI scanner. Randomly
51 presented auditory sounds (n=50) prompted subjects to evaluate and report their mental content as it was prior the probe.
52 Possible mental states were: i) MB, ii) perception of sensory stimuli without internal thoughts (Sens), iii) stimulus-dependent
53 thoughts (SDep), and iv) stimulus-independent thoughts (SInd). With this setup, Rest periods and Response-type periods could
54 be determined (Fig.1A).

55 Behavioral reports

56 We found that MB was reported significantly fewer times than any other mental state (median=2.5, IQR=3, min=0, max=9;
57 Fig.2A). There was a main effect of mental state with respect to reaction times ($\chi^2(3) = 66.63, p < 0.001$; generalized
58 linear mixed model analysis with gamma distribution and inverse link function), with MB being reported faster than SDep
59 ($z = 3.81, p = 0.0008$) and SInd ($z = 3.37, p = 0.0042$) but with no differences from Sens ($z = -0.73, p = 0.89$; post-hoc
60 Tukey test; Fig.2B). The evaluation of the dynamic transitions among different mental states showed exceptionally low, but
61 equal probabilities (0.06) of reporting MB departing from a content-oriented state. Inversely, departures from MB towards
62 content-oriented reports were characterized by high transition probabilities (>0.27). Also, the probability to re-enter MB (i.e.
63 reporting another MB immediately after a MB report) was particularly low (0.04, Fig.2C). Finally, the hypothesis for a uniform
64 distribution of reports across the session could not be rejected either for MB ($\chi^2(9) = 12.31, p = 0.20, \phi = 0.35$; Fig.2D) or
65 for SDep ($\chi^2(9) = 5.25, p = 0.81, \phi = 0.10$) and SInd ($\chi^2(9) = 4.22, p = 0.90, \phi = 0.07$). However, Sens reports were not
66 equally distributed over time ($\chi^2(9) = 18.15, p = 0.03, \phi = 0.23$).

67 Brain patterns and neurofunctional analysis

68 By means of phase-based coherence connectivity analysis and k-means clustering, we determined four brain patterns which
69 appeared recurrently across the rest periods (Fig.1B). The patterns were characterized by distinct signal configurations: a
70 pattern of complex inter-areal interactions, containing positive and negative phase coherence values between long-range
71 and short-range regions (Pattern 1), a pattern showing signal anti-correlations primarily between the visual network and the
72 other networks (Pattern 2), a pattern with overall positive inter-areal phase coherence (Pattern 3), and a pattern of overall
73 low inter-areal coherence (Pattern 4, Fig.3A). In terms of occurrences, Pattern 4 appeared at a significantly higher rate than
74 Pattern 1 ($t(35) = 6.23, p < 0.001$, Cohen's $d = 1.04$), Pattern 2 ($t(35) = 5.27, p < 0.001$, Cohen's $d = 0.88$) and Pattern 3
75 ($t(35) = 5.50, p < 0.001$, Cohen's $d = 0.92$, p-values are FDR corrected at $\alpha = 0.05$; Fig.3B).

To determine which brain pattern was the closest to MB reports, we used the cosine distance as the similarity measure between five connectivity matrices preceding a report (i.e., Response-type periods) and the four brain patterns (Fig. 1C). Using a generalized linear mixed model fit to the distance measures of each brain pattern separately, we found a significant effect of mental state for distance values to Pattern 3 ($\chi^2(3) = 15.47, p = 0.001$) and Pattern 4 ($\chi^2(3) = 8.83, p = 0.032$). Pattern 3 further showed higher similarity to MB compared to the reports about Sens (*Estimate* = 0.09, $z = 2.71, p = 0.034$), SDep (*Estimate* = 0.11, $z = 3.48, p = 0.003$), and SInd thoughts (*Estimate* = 0.12, $z = 3.82, p < 0.001$; Post-hoc tukey tests, Fig.4).

Information flow analysis

To determine each mental state's integration/segregation profile, we used diffusion maps followed by mental state classification. Diffusion-map analysis is a non-linear dimensionality reduction technique based on spectral graph theory²¹. Applied to brain data, a larger distance in the diffusion values between regions indicates smaller between-region transition probabilities, which implies that information exchange is less efficient. For each mental state report, diffusion maps were calculated on the average of response-type connectivity matrices related to that state. We found that for MB, diffusion values have larger distances between regions of the DMN (red range values) and what is broadly defined as the salient network (blue range values). Furthermore, the diffusion value distance was smaller for content-oriented reports (Fig.5A). Using subjects' maps as feature vectors and applying a C4.5 decision tree classifier with a 10-fold cross validation scheme, mental state classification was achieved at an accuracy of 81.16% (Table1 and Table2). Based on the classifier's optimum decision tree and the brain regions' diffusion values, the somatomotor network was the region whose diffusion value separated MB from thought-oriented reports (Fig.5B). Subsequently, the final classification between thought-oriented reports (SDep vs. SInd) was achieved with the contribution of DMN prefrontal regions. Similarly, MB classification was achieved when the diffusion value was <0.6 in the left fronto-insular cortex (salience network). When the diffusion value in this region was higher, the decision between MB and Sens reports required more steps and the contribution of right parietal areas, bilateral visual, and left temporal cortices (Fig.5B).

Discussion

We investigated the neurofunctional profile of mind blanking (MB) and found that it occupies a unique position among thought-oriented reports during spontaneous mentation. By means of experience-sampling within the fMRI environment, we first show that typical individuals have few number of MB reports, which are reported faster than other mental states. These findings are in line with previous studies showing that MB gets reported significantly less often than thought-related content²⁰. Our results are also in line with studies reporting similarly fast MB reaction times while participants are involved in sustained attention to response task^{7,22}. Nevertheless, in other investigations MB is reported more slowly compared to other mental states, which is interpreted as MB facilitating sluggishness in responses²³ or as the result of decreases in alertness and arousal during task performance⁵. Here, we consider that the fast reaction times for MB and the longer reaction times for thought-oriented reports (SDep, SInd) might be attributed to an additional cognitive evaluation of the latter. In other words, when thoughts are occupied by content, they are translated in longer cognitive evaluation as to the particularities of their content. In that

108 respect, MB, being defined as content-free state, is reported faster. This interpretation supports previous investigations using
109 self-paced focused reading with self-catches of MB and mind wandering, which tested how these mental modes affect reading
110 comprehension³.

111 Regardless of this heterogeneity, it can be generally concluded that MB gets reported despite its content-less phenomenology.
112 Therefore, MB can be considered as one more mental state which contributes to spontaneous mentation. Its role among the
113 content-oriented states is here determined by the performed dynamic analysis. We show that the probabilities in reporting
114 MB (after reporting another state) are low, but equal. At the same time, departures from MB are more likely to lead toward
115 content-oriented thoughts, and less likely to lead towards MB again. Collectively, these results indicate that MB might not be
116 driven by any specific mental content, therefore serving as a transient mental relay²⁴. In other words, thoughts with content can
117 lead towards more mental contents due to semantic associations, hence creating the perception of a stream of consciousness.
118 Since MB is not semantically associated with any particular mental content, it does not occur frequently during spontaneous
119 thinking. As such, phenomenologically content-less reports might have less of an anchoring effect than content-full reports.
120 The eventual finding of a uniform distribution of MB reports over time, also reported elsewhere^{3,25}, further suggests that MB is
121 not a result of fatigue, and therefore confirms its unique place as a default mental state during spontaneous mentation.

122 By investigating whole-brain time-varying functional connectivity during the resting periods of the experience-sampling
123 task, we show four distinct brain patterns occurring across time. These brain patterns bear great resemblance with what we
124 previously reported as recurrent brain configurations during pure resting state fMRI acquisitions across healthy individuals
125 and brain-injured patients¹⁵. The fact that these patterns appear across independent datasets, and that they are present also in
126 non-human primates²⁶, utilizing different paradigms and different brain parcellations, points to their universality and robustness.
127 Our finding that Pattern 4 (low inter-areal connectivity) shows the highest occurrence probability in comparison to the other
128 patterns, is explained by the fact that this configuration has the highest similarity to the underlying structural connectome¹⁵. As
129 such, this pattern may act as a foundation upon which the others can occur, by showing divergence of function from structure,
130 which is linked to mental flexibility²⁷. On the other hand, an all-to-all positive inter-areal connectivity has the lowest occurrence
131 probability and high similarity to the connectivity matrices preceding MB reports. This global inter-region positive connectivity
132 has been previously reported to occur with high prevalence in NREM slow-wave sleep^{28,29}. In this sleep stage, the brain's slow
133 wave activity reflects minimal neuronal firing. Studies in rats¹⁹ show that periods of neuronal silencing can happen also during
134 wakefulness in the form of neuronal firing rate reduction leading to slow wave activity, which was indicative of local sleeps.
135 When applied to humans, it has been argued that these instances of local sleeps can be the phenomenological counterpart
136 of MB²³. In that respect, wakefulness is not a physiological state of constantly on-periods of neuronal function. Rather, the
137 fact that our brains show instances of neural down-states even during wakefulness possibly for homeostatic reasons³⁰, can be
138 neurally translated as global positive connectivity and phenomenologically interpreted as MB.

139 This possibility is further accounted by prominent theoretical models of conscious experience. The Global Neuronal
140 Workspace Theory (GNWT)³¹ posits that a stimulus becomes reportable when some of its locally processed information

141 becomes available to a wide range of brain regions, forming a balanced distributed network³². Therefore, the brain in a
142 state of all-to-all positive connectivity provides not some, but all of its locally processed information globally so that, for
143 a moment, no information is in a privileged state of processing and available to attention and awareness. This can also be
144 similarly explained in the context of the supervisory attentional system (SAS)²⁵, whose all "action systems" (i.e. processing
145 structures associated with particular tasks) will have the same dominance, leaving the SAS unable to choose which one to
146 bring into awareness. This lack of differentiation is also portrayed in the Integrated Information Theory (IIT¹⁶). According
147 to this theory, to generate an experience a physical system must be able to discriminate among a large repertoire of states
148 (i.e., information). This must be done as a single system that cannot be decomposed into a collection of causally independent
149 parts (i.e., integration). The all-to-all positive connectivity pattern is characterized by the highest level of integration and
150 efficiency and the lowest level of segregation and modularity compared to the other brain patterns¹⁵. Therefore, it is implied
151 that such a neural configuration is unable to produce high values of integrated information, leading to limited experience. Here,
152 information flow was approximated by the diffusion-map analysis. Before MB reports, we observed a large range of diffusion
153 values between DMN and other areas, which is indicative of low between-node transition probabilities. Therefore, MB is linked
154 to rigid and inefficient information exchange. Such inefficient information flow between the DMN and other networks has also
155 been reported while participants were instructed to think of nothing⁸. Finally, with respect to the left fronto-insular area (part of
156 the salience network), we found that this region predicted MB reports when it was highly segregated from the DMN early and
157 in few steps during the classification scheme. The involvement of the salience network does not come as a surprise. Indeed, this
158 system has been shown to play an important role in switching between the DMN and the central executive network (CEN),
159 making salient and important stimuli available to the focus of attention³³. Also recently, it is shown that prestimulus activity of
160 anterior insula predicts the conscious perception of visual stimuli, so that this region might act as a gate for conscious access³⁴.
161 In a similar line, as MB is free of phenomenological content, it can be that its saliency evaluation happens effortlessly and early
162 on during the neurocognitive hierarchy translated in a more laxed inter-network engagement.

163 Our study is limited in several ways. First, the experience-sampling task utilized a probe-catching methodology. This means
164 that participants were interrupted during spontaneous thinking by a probe, asking them to choose an appropriate report option to
165 describe their thought-state. Such a probe-framing technique can restrict the estimation of potential phenomenological switches
166 happening between the probes. Indeed, as the probes were appearing in pre-determined time points we cannot exclude the
167 possibility of mental contents happening during the inter-probe intervals, and hence they were missed to be reported. Also,
168 probe-framing can be suboptimal in capturing spontaneous thinking because it might lead to an inflated number of MB reports.
169 This is because participants could choose this category since it was pre-established, which they could otherwise not report if they
170 were to identify spontaneously³⁵. The fact, though, that MB occurrences were not reported with a comparable high frequency
171 to the content-oriented states might indicate that MB was evaluated in a representative way across the evaluation, leading to
172 infrequent occurrences across participants. This small number of MB reports, in turn, could be considered problematic in
173 terms of statistical inference. To address this issue, the analysis referred to data which were concatenated across subjects. This

174 technique on the one hand increased the number of MB reports in our statistical models. On the other hand, this solution might
175 have influenced the between-subject variability, which was here mitigated by assuming subjects as random effects variable in
176 the mixed effect analysis. Finally, the high TR during the fMRI acquisition (2.04s) could also echo the temporal implications of
177 the MB profiling. By means of simultaneous EEG-fMRI recordings, more light is expected to be shed on fine-grained temporal
178 dynamics of MB. Such simultaneous multi-modal recordings are expected to also illuminate the assumption of slow-wave
179 activity as the corresponding neural mechanism of MB. In the absence of vigilance monitoring with EEG or pupil diameter, this
180 hypothesis remains to be further tested.

181 In conclusion, our study suggests that MB can be considered as a default mental state occupying a unique position among
182 content-oriented thoughts. Its rigid neurofunctional profile could account for the inability to report mental content due to the
183 brain's inability to configure complex inter-areal dynamics. The DMN-salience network segregation which appears to lead
184 towards MB reporting, paves the way to more mechanistic explorations of MB. Collectively, MB's unique neurofunctional
185 profile among thought-oriented reports supports the view that instantaneous mental absences can happen during wakefulness,
186 setting this mental state at a prominent phenomenological position during ongoing mentation.

187 Methods

188 Participants

189 Participants were healthy right-handed adults who were French speaking, university students or graduates with at least a high
190 school diploma without psychiatric or neurological disorders. All subjects gave their written informed consent to take part in
191 the experiment and ethics committee of the University Hospital of Liège approved the study.

192 Experience-sampling task

193 Setup and procedure

194 Participants were lying restfully in the scanner with eyes open. At random times, they were interrupted by an auditory tone,
195 probing them to report their immediate mental state via button presses. The sampling probes were randomly distributed between
196 30 and 60 seconds. Each probe started with the appearance of an exclamation mark lasting for 1000 ms inviting the participants
197 to review and characterize the cognitive event(s) they just experienced. Several screens were presented in succession so
198 participants could communicate their mental state type. The first screen offered four categories for a broad characterization
199 of the cognitive experience: Absence, Perception, Stimulus-dependent thought, and Stimulus-independent thought. Absence
200 was defined as mind blanking or empty state of mind. Perceptions represented the acknowledgment of a stimulus through
201 one or more senses without any internal thought. Thoughts were distinguished as stimulus-dependent (i.e. with awareness of
202 the immediate environment), or stimulus-independent (i.e. with no awareness of the immediate environment). For reporting,
203 participants used two response boxes, one in each hand. Participants used an egocentric mental projection of their fingers onto
204 the screen so that each finger corresponded to a specific mental category. Depending on the probes' trigger times and reaction
205 times, the duration of the recording session was variable (48–58 min) across subjects. To minimize misclassification rates,

206 participants had a training session outside of the scanner at least 24 hours before the actual session.

207 ***Behavioral statistical analysis***

208 Analyses were performed using locally developed codes in Python and R. Six paired t-tests were used to analyze the occurrence
209 number of each mental state (p-values were FDR-corrected with a significance level of $\alpha = 0.05$). A generalized linear mixed
210 model with a gamma distribution and inverse link function tested the relationship between reaction times and mental states.
211 Mental state reports were considered as fixed effects and participants were considered as the random effects with sex and age as
212 confound variables. In case of significant main effects, post-hoc Tukey pairwise comparisons were applied. To model dynamic
213 relationship between mind states, a Markov model was used to calculate the transition probabilities between participants'
214 reports over the experiment. The uniformity of the distribution of each report over the acquisition duration was tested using
215 the χ^2 test on the report times across all participants. The acquisition duration of each subject was divided into 10 equal time
216 bins and number of reports at each bin was counted. To calculate the effect size of the χ^2 test, ϕ measure was used ($\phi = \sqrt{\frac{\chi^2}{n}}$,
217 where n is the number of observations).

218 **Neuroimaging**

219 ***MRI acquisition***

220 Experiments were carried out on a 3-T head-only scanner (Magnetom Allegra, Siemens Medical Solutions, Erlangen, Germany)
221 operated with the standard transmit–receive quadrature head coil. fMRI data were acquired using a T2*-weighted gradient-echo
222 EPI sequence with the following parameters: repetition time (TR) = 2040 msec, echo time (TE) = 30 msec, field of view
223 (FOV) = $192 \times 192 \text{ mm}^2$, 64 × 64 matrix, 34 axial slices with 3 mm thickness and 25% interslice gap to cover most of the
224 brain. The three initial volumes were discarded to avoid T1 saturation effects. Field maps were generated from a double echo
225 gradient-recalled sequence (TR = 517 msec, TE = 4.92 and 7.38 msec, FOV = $230 \times 230 \text{ mm}^2$, 64 × 64 matrix, 34 transverse
226 slices with 3 mm thickness and 25% gap, flip angle = 90° , bandwidth = 260 Hz/pixel) and used to correct echo-planar images
227 for geometric distortion because of field inhomogeneities. A high-resolution T1-weighted MP-RAGE image was acquired
228 for anatomical reference (TR = 1960 msec, TE = 4.4 msec, inversion time = 1100 msec, FOV = $230 \times 173 \text{ mm}$, matrix size
229 = $256 \times 192 \times 176$, voxel size = $0.9 \times 0.9 \times 0.9 \text{ mm}$). The participant's head was restrained using a vacuum cushion to
230 minimize head movement. Stimuli were displayed on a screen positioned at the rear of the scanner, which the participant could
231 comfortably see using a head coil mounted mirror.

232 ***Preprocessing***

233 Preprocessing and denoising were performed using a locally developed, freely available online, pipeline written in Python
234 (nipype package³⁶) encompassing toolboxes from Statistical Parametric Mapping 12³⁷, FSL 6.0³⁸, AFNI³⁹, and ART (<http://web.mit.edu/swg/software.htm>; https://gitlab.uliege.be/S.Mortaheb/mind_blanketing/). All
235 the functional volumes were realigned to the first volume and then, in a second pass, to their average. Estimated motion
236 parameters were then used for artifact detection using ART toolbox. An image was defined as an outlier or artifact image if the
237

238 head displacement in the x, y, or z direction was greater than 3 mm from the previous frame, if the rotational displacement was
239 greater than 0.05 rad from the previous frame, or if the global mean intensity in the image was greater than 3 SDs from the
240 mean image intensity for the entire scans. After skull-stripping of structural data (using FSL BET⁴⁰ with fractional intensity
241 of 0.3), realigned functional images were registered to the bias-corrected structural image in the subject space (rigid-body
242 transformation with normalized mutual information cost function). After extracting white matter (WM), grey matter (GM), and
243 cerebrospinal fluid (CSF) masks, all the data and masks were transformed into the standard stereotaxic Montreal Neurological
244 Institute (MNI) space (MNI152 with 2 mm resolution). WM and CSF masks were further eroded by one voxel. For noise
245 reduction, we modeled the influence of noise as a voxel specific linear combination of multiple empirically estimated noise
246 sources by deriving the first five principal components from WM and CSF masked functional data separately. These nuisance
247 regressors together with detected outlier volumes, motion parameters and their first-order derivative were used to create a design
248 matrix in the first-level general linear model (GLM). After smoothing the functional data using a Gaussian kernel of 6-mm full
249 width at half-maximum, the designed GLM was fitted to the data. Before applying GLM, functional data were demeaned and
250 detrended and all the motion-related and tissue-based regressors were first normalized and then demeaned and detrended using
251 the approach explained in⁴¹. A temporal bandpass filter of 0.008 to 0.09 Hz was then applied on the residuals of the model
252 to extract low frequency fluctuations of the BOLD signal. Schaefer atlas⁴² with 100 ROIs were then used to parcellate each
253 individual brain. Average of voxel time series in each region was considered as the extracted ROI time series and were used for
254 further analysis.

255 **Functional connectivity matrices**

We used the phase-based coherence to extract between-region connectivity patterns at each time point of the scanning sessions¹⁵. For each subject i , after z-normalization of time series at each region r (i.e. $x_{i,r}(t)$), the instantaneous phase of each time series were calculated using Hilbert transform. However, in order to have a more accurate estimate of the instantaneous phase, a narrower bandpass filter was applied on the time series (Second order Butterworth filter in range [0.01-0.04] Hz), and then the Hilbert transform was applied on the time series as:

$$\hat{x}_{i,r}(t) = \frac{1}{\pi t} * x_{i,r}(t), \quad (1)$$

in which $*$ indicates a convolution operator. Using this transformation, an analytical signal was produced for each regional time series as:

$$X_{i,r}^a(t) = x_{i,r}(t) + i\hat{x}_{i,r}(t). \quad (2)$$

From this analytical signal, the instantaneous phase of each time series can be estimated as:

$$\phi_{i,r}(t) = \angle X_{i,r}^a(t) = \tan^{-1}\left(\frac{\hat{x}_{i,r}(t)}{x_{i,r}(t)}\right). \quad (3)$$

After wrapping each instantaneous phase signal of $\phi_{i,r}(t)$ to the $[-\pi, \pi]$ interval and naming the obtained signal as $\theta_{i,r}(t)$, a connectivity measure for each pair of regions was calculated as the cosine of their phase difference. For example, the connectivity measure between regions r and s in subject i was defined as:

$$conn_{i,r,s}(t) \triangleq \cos(\theta_{i,r}(t) - \theta_{i,s}(t)). \quad (4)$$

By this definition, completely synchronized time series lead to have a connectivity value of 1, completely desynchronized time series produce a connectivity value of zero, and anti-correlated time series produce a connectivity measure of -1. Using this approach, a connectivity matrix of 100×100 was created at each time point t of each subject i that we called it $C_i(t)$:

$$C_i(t) \triangleq [conn_{i,r,s}(t)]_{r,s}. \quad (5)$$

256 After collecting connectivity matrices of all time points of all participants, k-means clustering was applied on the matrices
257 just related to the resting parts of the experiment. With this technique, four robust and reproducible patterns were extracted as
258 the centroids of the clusters and each resting connectivity matrix was assigned to one of the extracted patterns. The occurrence
259 rate of each pattern was simply calculated by counting the number of matrices which were assigned to each specific pattern at
260 each subject separately. Significant differences between patterns occurrence rates were analyzed using paired t-test and FDR
261 correction of p-values over six possible pairwise comparisons.

262 **Neurofunctional analysis**

To evaluate the similarity between mental states' functional connectivity patterns and the four main resting state recurrent functional configurations, we extracted the five connectivity matrices preceding each probe (as the functional repertoire of each specific mental state) and then calculated their cosine distance to the four main resting state patterns. Cosine distance between two sample matrices of A and B can be calculated as:

$$dist(A, B) = \frac{Tr(A^T B)}{\sqrt{Tr(A^T A)Tr(B^T B)}}, \quad (6)$$

263 where $Tr(.)$ indicates trace of a matrix. Subsequently, for each mental state the distribution of distances to all four centroids
264 were created. A generalized linear mixed effect model with gamma distribution and log link function was applied to test the
265 relationship between the distances to each pattern and the mental states. In this model, mental state reports were considered as
266 fixed effects and participants as random effects with sex and age as confound variables.

267 **Diffusion maps**

268 Diffusion-map analysis is a non-linear dimensionality reduction technique based on spectral graph theory²¹ that checks the
269 information flow between nodes based on the transition probabilities denoted by the connection weight between the nodes.
270 The resulting diffusion map summarizes that the larger the distance in the diffusion values between regions, the smaller the

271 transition probability, which indicates less efficient information exchange.

272 To extract diffusion map of a sample connectivity matrix, the following steps were taken:

273

274 • For connectivity matrix $W_{100 \times 100}$, set all the negative weights to zero.

275 • Define a diagonal matrix (node strength) $D_{100 \times 100}$, such that $D_{ii} = \sum_{j=1}^{100} W_{ij}$

276 • Create the transition probability matrix $M_{100 \times 100}$, such that $M_{ij} = W_{ij}/D_{ii}$ (an asymmetric matrix denoting transition
277 probability from region i to region j)

278 • Create a symmetric matrix M_s with the same eigenvalues as M : $M_s = D^{1/2}MD^{-1/2}$

279 • Perform eigen decomposition on M_s to obtain its eigenvalues and corresponding orthonormal eigenvectors and sort them
280 from the largest eigenvalue to the smallest.

281 • Take the first eigenvector as the main diffusion map of the connectivity matrix.

282 In this study, diffusion maps were estimated for the averaged connectivity matrices of each mental state. For the subsequent
283 analysis, all the diffusion maps should also be aligned over the participants. Here, diffusion maps estimation and their alignment
284 over participants have been performed using an open source package (<https://github.com/satra/mapalign>)⁴³. As
285 in this package, a singular value decomposition (SVD) technique is used to align the estimated diffusion maps, and SVD result
286 is slightly different in various system configurations, we here report that in this study, diffusion map analysis were performed in
287 a MacBook Pro 2018 TOUCH BAR MV962, processor Intel Core i5-8269U, using Python version 3.7.4 and Numpy version
288 1.17.2.

289 **Mental state classification**

290 Estimated diffusion maps were used as feature vectors and a C4.5 decision tree classifier⁴⁴ was used to classify mental states
291 based on diffusion maps. This is a very efficient algorithm for representation of rule classification which locates the most
292 robust features for the initial separation of the dataset, and then selects potential subtrees affected by noisy features, and
293 prunes them. The pruned features are removed from the initial dataset and C4.5 re-runs since there is an improvement on
294 the classification accuracy. In this study, the J48 (a Java implementation of C4.5 Classifier) decision tree, implemented in
295 the Waikato Environment for Knowledge Analysis (WEKA)⁴⁵ was employed. The confidence factor (C) was set to 0.25 and
296 the minimum number of instances per leaf (M) was set to 3. Classification accuracy was computed using the 10-fold cross
297 validation strategy. According to this strategy, the dataset is divided into ten non-overlapping subsets (folds), where nine are
298 used for training and one for testing. Accuracy is then defined as the ratio of the correctly classified instances divided by the
299 total number of instances. To minimize the sampling bias, this procedure is repeated 10 times so each subset serves as a testing
300 set and the model's overall accuracy is defined as the average of the 10 single-fold accuracies.

301 Acknowledgements

302 This work was supported by Belgian Fund for Scientific Research (FNRS). S.Mortaheb is a Research Fellow, A.Demertzis a
303 Research Associate, and S.Majerus is a Research Director at the FNRS. We also thank Mr Larry D. Fort for proof reading and
304 editing the manuscript.

305 Author contributions statement

306 S.Mortaheb and A.D. conducted the research and wrote the manuscript. S.Mortaheb performed behavioral and neurofunctional
307 data analysis. M.A.K. performed information flow analysis. P.A.B., K.G., and S.Mortaheb performed article review. L.V.C. and
308 S.Majerus acquired the experience-sampling dataset. All authors reviewed the manuscript.

309 Additional information

310 **Accession codes:** All the codes used to generate results in this manuscript are accessible online via:

311 https://gitlab.uliege.be/S.Mortaheb/mind_blankng. The dataset used in the analysis is freely accessible via the OSF page of
312 the project: <https://osf.io/gwrtc/>

313 **Competing interests:** The authors declare no competing interests.

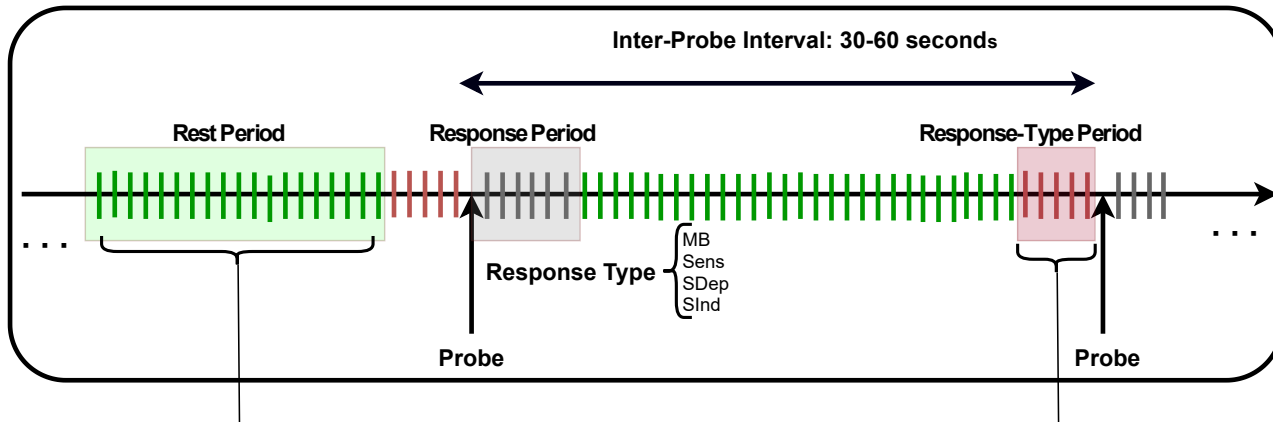
314 References

- 315 1. Smallwood, J. *et al.* The neural correlates of ongoing conscious thought. *Iscience* **102132** (2021).
- 316 2. Winter, U. *et al.* Content-free awareness: Eeg-fcmri correlates of consciousness as such in an expert meditator. *Front.*
Psychol. **10** (2019).
- 317 3. Ward, A. F. & Wegner, D. M. Mind-blanking: When the mind goes away. *Front. psychology* **4**, 650 (2013).
- 318 4. Schooler, J. W. Zoning out while reading: Evidence for dissociations between experience and metaconsciousness jonathan
319 w. schooler, erik d. reichle, and david v. halpern. *Think. seeing: Vis. metacognition adults children* **203** (2004).
- 320 5. Unsworth, N. & Robison, M. K. Pupillary correlates of lapses of sustained attention. *Cogn. Affect. & Behav. Neurosci.* **16**,
321 601–615 (2016).
- 322 6. Van den Driessche, C. *et al.* Attentional lapses in attention-deficit/hyperactivity disorder: Blank rather than wandering
323 thoughts. *Psychol. science* **28**, 1375–1386 (2017).
- 324 7. Stawarczyk, D., François, C., Wertz, J. & D'Argembeau, A. Drowsiness or mind-wandering? fluctuations in ocular
325 parameters during attentional lapses. *Biol. Psychol.* **156**, 107950 (2020).
- 326 8. Kawagoe, T., Onoda, K. & Yamaguchi, S. Different pre-scanning instructions induce distinct psychological and resting
327 brain states during functional magnetic resonance imaging. *Eur. J. Neurosci.* **47**, 77–82 (2018).
- 328 9. Kawagoe, T., Onoda, K. & Yamaguchi, S. The neural correlates of “mind blanking”: When the mind goes away. *Hum.*
329 *brain mapping* **40**, 4934–4940 (2019).
- 330 10. Christoff, K., Irving, Z. C., Fox, K. C., Spreng, R. N. & Andrews-Hanna, J. R. Mind-wandering as spontaneous thought: A
331 dynamic framework (2016).
- 332 11. Alavash, M., Thiel, C. M. & Gießing, C. Dynamic coupling of complex brain networks and dual-task behavior. *NeuroImage*
333 **129**, 233–246 (2016).
- 334 12. Jobst, B. M. *et al.* Increased stability and breakdown of brain effective connectivity during slow-wave sleep: mechanistic
335 insights from whole-brain computational modelling. *Sci. Reports* **7**, 1–16 (2017).
- 336 13. Barttfeld, P. *et al.* Signature of consciousness in the dynamics of resting-state brain activity. *Proc. Natl. Acad. Sci.* **112**,
337 887–892 (2014). [arXiv:1408.1149](https://arxiv.org/abs/1408.1149).
- 338 14. Lutti, A. I. *et al.* Consciousness-specific dynamic interactions of brain integration and functional diversity. *Nat. Commun.*
339 **10**, 1–12 (2019).
- 340 15. Demertzi, A. *et al.* Human consciousness is supported by dynamic complex patterns of brain signal coordination. *Sci.*
341 *advances* **5**, eaat7603 (2019).
- 342 16. Tononi, G. Consciousness as integrated information: A provisional manifesto. *Biol. Bull.* **215**, 216–242 (2008).

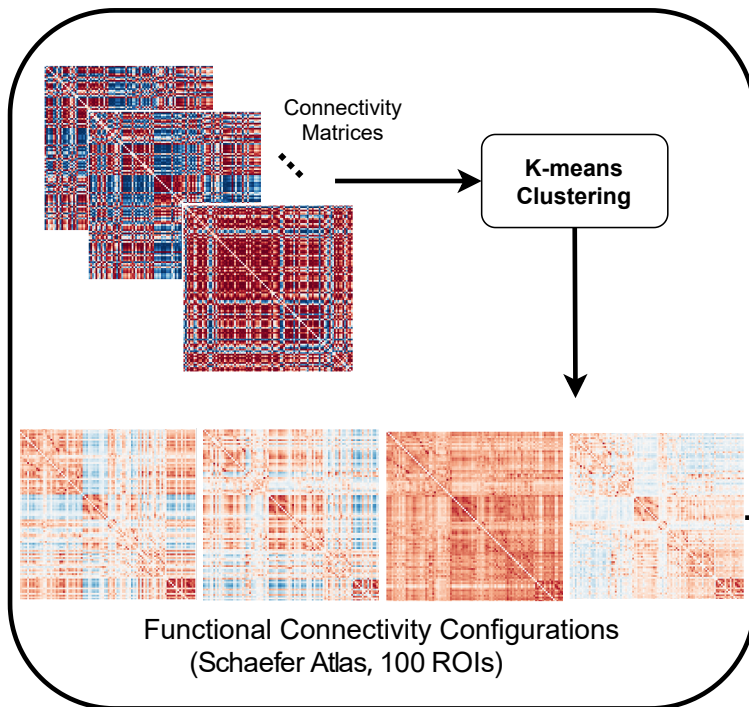
- 344 17. Dehaene, S., Sergent, C. & Changeux, J.-P. A neuronal network model linking subjective reports and objective physiological
345 data during conscious perception. *Proc. Natl. Acad. Sci.* **100**, 8520–5 (2003).
- 346 18. Blumenfeld, H. Impaired consciousness in epilepsy. *The Lancet Neurol.* **11**, 814–826 (2012). [NIHMS150003](#).
- 347 19. Vyazovskiy, V. V. *et al.* Local sleep in awake rats. *Nature* **472**, 443–447 (2011).
- 348 20. Van Calster, L., D'Argembeau, A., Salmon, E., Peters, F. & Majerus, S. Fluctuations of attentional networks and default
349 mode network during the resting state reflect variations in cognitive states: evidence from a novel resting-state experience
350 sampling method. *J. Cogn. Neurosci.* **29**, 95–113 (2017).
- 351 21. Coifman, R. R. *et al.* Geometric diffusions as a tool for harmonic analysis and structure definition of data: Diffusion maps.
352 *Proc. national academy sciences* **102**, 7426–7431 (2005).
- 353 22. Stawarczyk, D. & D'Argembeau, A. Conjoint influence of mind-wandering and sleepiness on task performance. *J.*
354 *experimental psychology: human perception performance* **42**, 1587 (2016).
- 355 23. Andrillon, T., Burns, A., MacKay, T., Windt, J. & Tsuchiya, N. Wandering minds, sleepy brains: lapses of attention and
356 local sleep in wakefulness. *bioRxiv* (2020).
- 357 24. Fornito, A., Harrison, B. J., Zalesky, A. & Simons, J. S. Competitive and cooperative dynamics of large-scale brain
358 functional networks supporting recollection. *Proc. Natl. Acad. Sci.* **109**, 12788–93 (2012).
- 359 25. Watts, F. N., MacLeod, A. K. & Morris, L. Associations between phenomenal and objective aspects of concentration
360 problems in depressed patients. *Br. J. Psychol.* **79**, 241–250 (1988).
- 361 26. Barttfeld, P. *et al.* Signature of consciousness in the dynamics of resting-state brain activity. *Proc. Natl. Acad. Sci.* **112**,
362 887–892 (2015).
- 363 27. Medaglia, J. D. *et al.* Functional alignment with anatomical networks is associated with cognitive flexibility. *Nat. Hum.*
364 *Behav.* **2**, 156–164 (2018). [1611.08751](#).
- 365 28. Aedo-Jury, F., Schwalm, M., Hamzehpour, L. & Stroh, A. Brain states govern the spatio-temporal dynamics of resting-state
366 functional connectivity. *Elife* **9**, e53186 (2020).
- 367 29. El-Baba, M. *et al.* Functional connectivity dynamics slow with descent from wakefulness to sleep. *PloS one* **14**, e0224669
368 (2019).
- 369 30. Bridi, M. C. *et al.* Daily oscillation of the excitation-inhibition balance in visual cortical circuits. *Neuron* **105**, 621–629.e4
370 (2020).
- 371 31. Dehaene, S., Changeux, J.-P., Naccache, L., Sackur, J. & Sergent, C. Conscious, preconscious, and subliminal processing:
372 a testable taxonomy. *Trends Cogn. Sci.* **10**, 204–211 (2006).
- 373 32. Sergent, C. & Dehaene, S. Neural processes underlying conscious perception: experimental findings and a global neuronal
374 workspace framework. *J. Physiol.* **98**, 374–384 (2004).

- 375 33. Menon, V. & Uddin, L. Q. Saliency, switching, attention and control: a network model of insula function. *Brain structure*
376 *function* **214**, 655–667 (2010).
- 377 34. Huang, Z. *et al.* Anterior insula regulates brain network transitions that gate conscious access. *Cell Reports* **35**, 109081
378 (2021).
- 379 35. Weinstein, Y., De Lima, H. J. & van der Zee, T. Are you mind-wandering, or is your mind on task? The effect of probe
380 framing on mind-wandering reports. *Psychon. Bull. Rev.* **25**, 754–760 (2018).
- 381 36. Gorgolewski, K. *et al.* Nipype: a flexible, lightweight and extensible neuroimaging data processing framework in python.
382 *Front. neuroinformatics* **5**, 13 (2011).
- 383 37. Penny, W. D., Friston, K. J., Ashburner, J. T., Kiebel, S. J. & Nichols, T. E. *Statistical parametric mapping: the analysis of*
384 *functional brain images* (Elsevier, 2011).
- 385 38. Jenkinson, M., Beckmann, C. F., Behrens, T. E., Woolrich, M. W. & Smith, S. M. Fsl. *Neuroimage* **62**, 782–790 (2012).
- 386 39. Cox, R. W. Afni: software for analysis and visualization of functional magnetic resonance neuroimages. *Comput. Biomed.*
387 *research* **29**, 162–173 (1996).
- 388 40. Smith, S. M. Fast robust automated brain extraction. *Hum. brain mapping* **17**, 143–155 (2002).
- 389 41. Power, J. D. *et al.* Methods to detect, characterize, and remove motion artifact in resting state fmri. *Neuroimage* **84**,
390 320–341 (2014).
- 391 42. Schaefer, A. *et al.* Local-global parcellation of the human cerebral cortex from intrinsic functional connectivity mri. *Cereb.*
392 *cortex* **28**, 3095–3114 (2018).
- 393 43. Langs, G., Golland, P. & Ghosh, S. S. Predicting activation across individuals with resting-state functional connectivity
394 based multi-atlas label fusion. In *International Conference on Medical Image Computing and Computer-Assisted*
395 *Intervention*, 313–320 (Springer, 2015).
- 396 44. Quinlan, J. R. C4. 5: Programs for machine learning. san francisco, ca, usa, 1993.
- 397 45. Frank, E., Hall, M. A. & Witten, I. H. *The WEKA workbench* (Morgan Kaufmann, 2016).

(A) Experience-Sampling Paradigm



(B) Resting State Pattern Extraction



(C) Neurofunctional Analysis

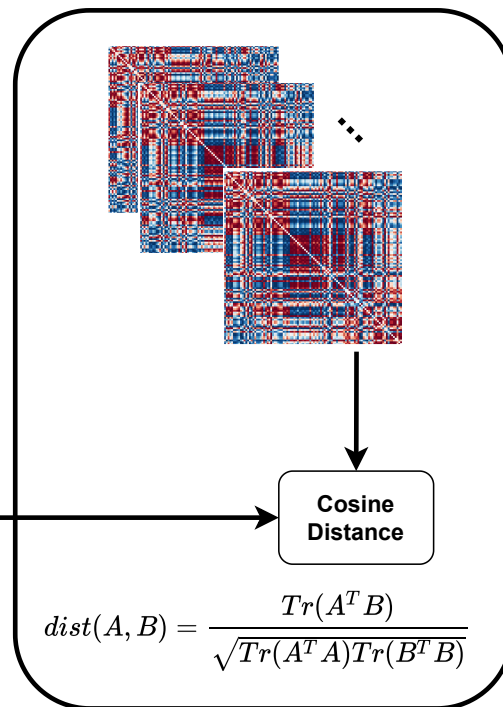


Figure 1. Experience-sampling task and analysis pipeline. (A) Participants' resting state was interrupted by auditory probes, inviting them to evaluate and report their mental state as this was before the probe, choosing among four pre-defined options (Response-types). (B) For brain pattern extraction, phase-based coherence was first used to estimate scan-wise connectivity matrices during the Rest Periods of the paradigm (green-shaded scans). Then, unsupervised machine learning with k-means estimated variant emerging signal configurations, which could recurrently appear across the acquisition. (C) To determine which brain pattern supported the reported mental states, a similarity measure was used, which compared the cosine distance between the five connectivity matrices preceding each report (red-shaded scans, Response-type periods) and the previously emerged brain patterns.

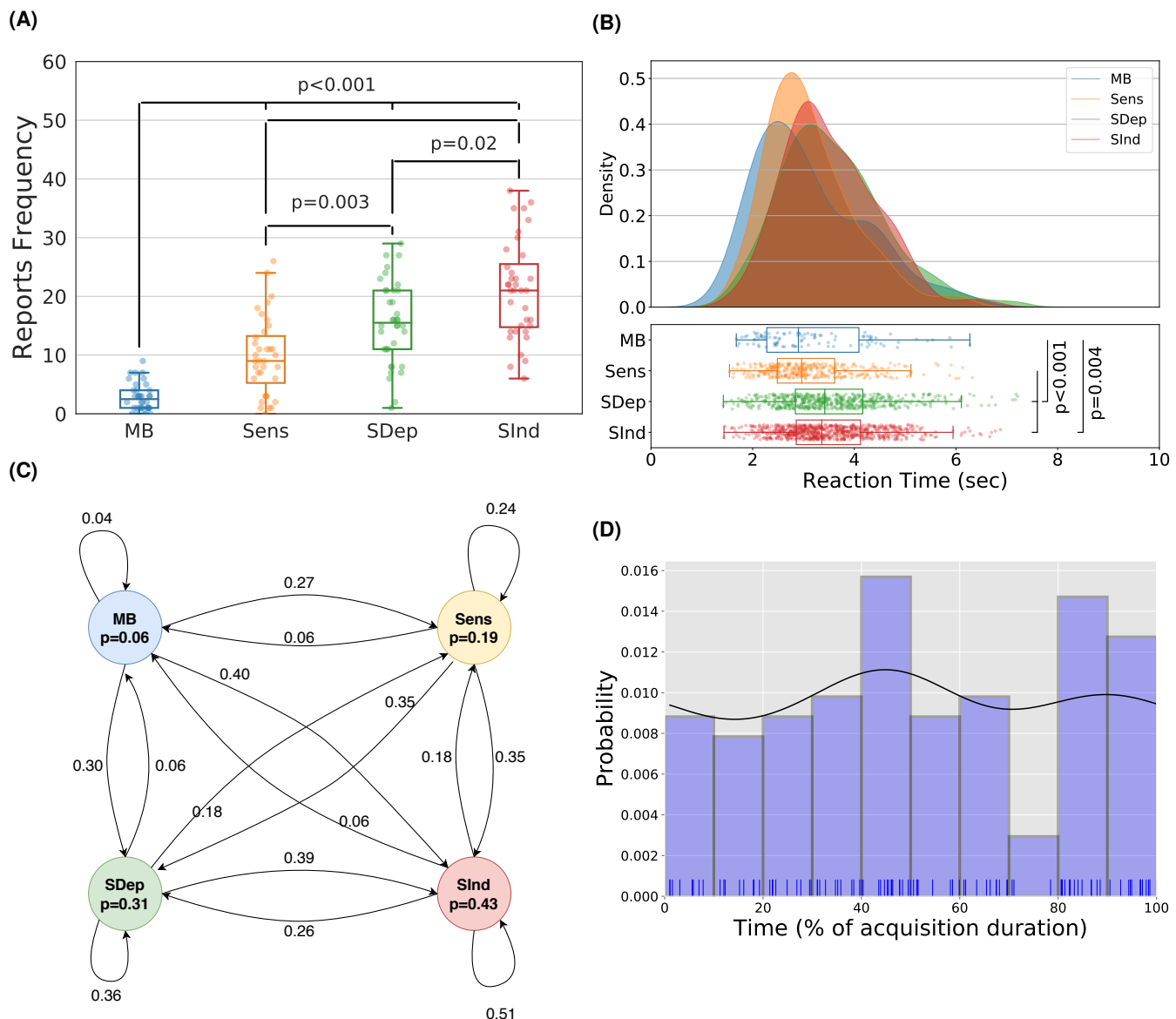
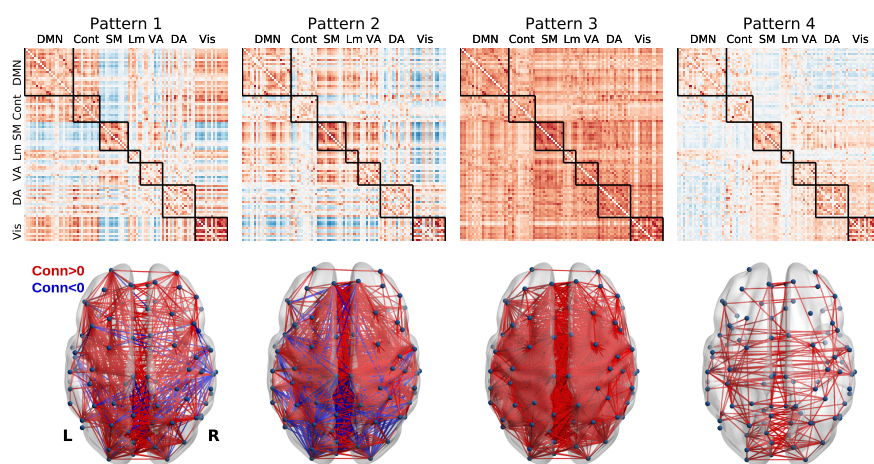


Figure 2. Mind blanking occupies a unique position among content-oriented reports. (A) Participants reported significantly fewer MB events than sensory-oriented (Sens), stimulus-dependent (SDep) and stimulus-independent (SInd) thoughts, confirming the less frequent yet non-negligible occurrence of MB across time (paired t-tests, FDR corrected at $\alpha = 0.05$). (B) Thought-oriented reports (SDep, SInd) had longer reaction times than MB and sensory-related reports, potentially due to a second-level cognitive evaluation of mental content that stimulus-related thoughts necessitated before reporting (generalized linear mixed effect model, adjusted p-values at $p < 0.05$). (C) The probability of reporting MB was low yet equal when departing from content-oriented states (markov chain modelling; numbers indicate transition probability matrix values). Also, the particularly low likelihood to re-enter MB indicates that MB might not be driven by specific mental content, hence serving as a transient mental relay. (D) The distribution of MB reports follows a uniform shape, indicating that MB occurrences spread equally over time and therefore may comprise a default mental state. Notes: catplots represent count, boxplots represent medians with interquartile range (25th-75th percentile), histogram with 10 bins related to the equal divisions of experiment duration to its 10% time slots.

(A)



(B)

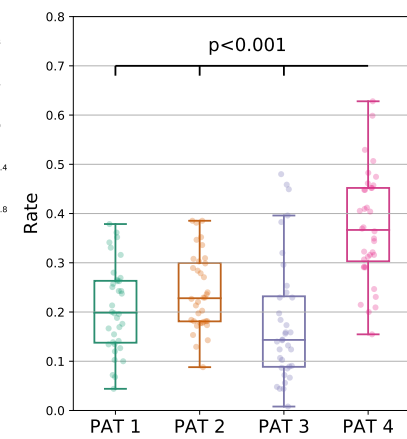


Figure 3. Four distinct signal configurations were recurrently present across resting periods. (A) Pattern 1 showed complex inter-areal functional configurations, characterized by short- and long-range connectivity, of positive and negative valence. Pattern 2 showed mainly functional anti-correlations between visual areas and regions of other networks. Pattern 3 showed all-to-all positive functional connectivity among the areas of the studied networks. Pattern 4 showed overall low inter-areal connectivity. (B) When estimating each pattern's occurrence rate, Pattern 4 had significantly the highest probability to appear across the resting periods while Pattern 3 had the lowest (paired t-tests, FDR corrected at $\alpha = 0.05$). Brain regions are organized in networks as indicated by the Schaefer atlas; 100 regions (DMN: Default Mode Network, Cont: Executive Control Network, SM: Somatomotor, Lm: Limbic, VA: Ventral Attentional, DA: Dorsal Attentional, Vis: Visual). Colorbar indicates coherence values between any pair of regions.

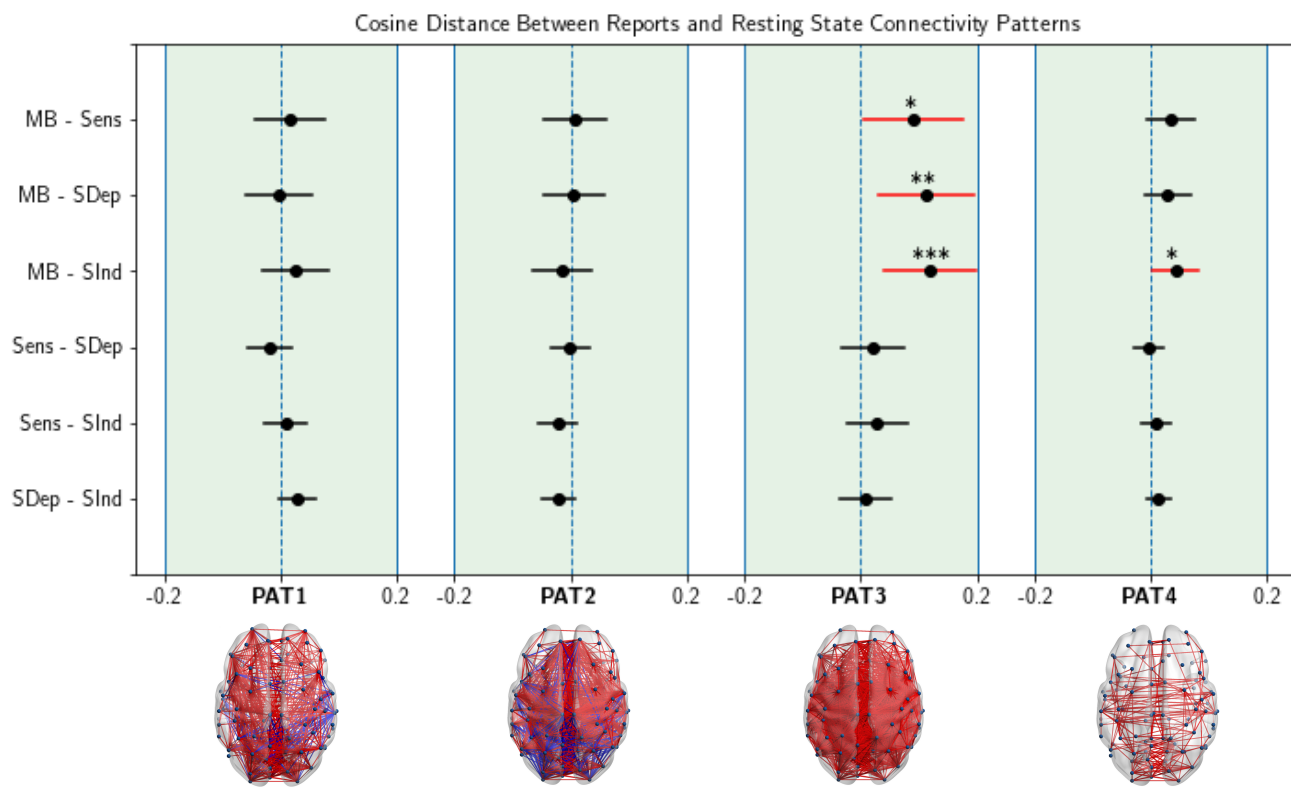
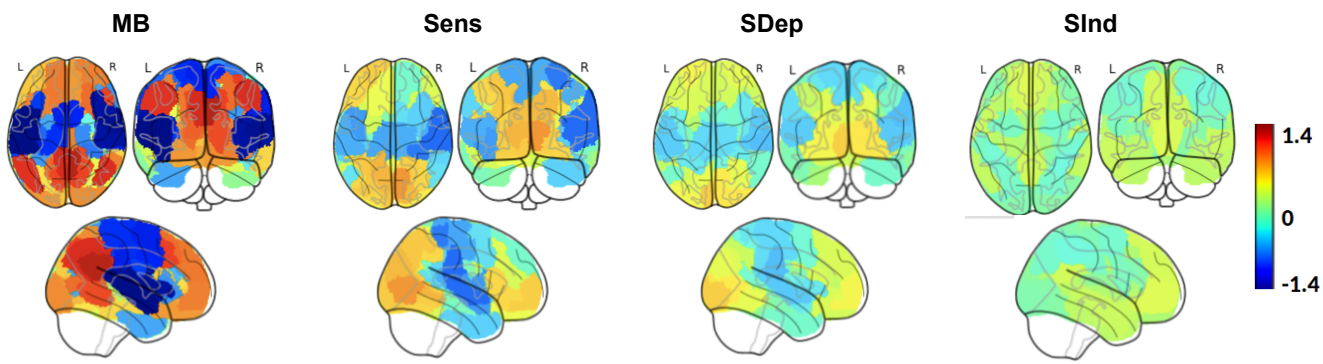


Figure 4. The positive all-to-all inter-areal connectivity pattern was the most similar configuration to MB reports. There was a significant effect of mental state on the distance values to Pattern 3 and Pattern 4. Post-hoc tukey test showed that MB had the highest similarity to Pattern 3 in comparison to all other mind states (error bars indicate asymptomatic confidence intervals around the difference estimate, * $p<0.05$, ** $p<0.01$, *** $p<0.001$).

(A)



(B)

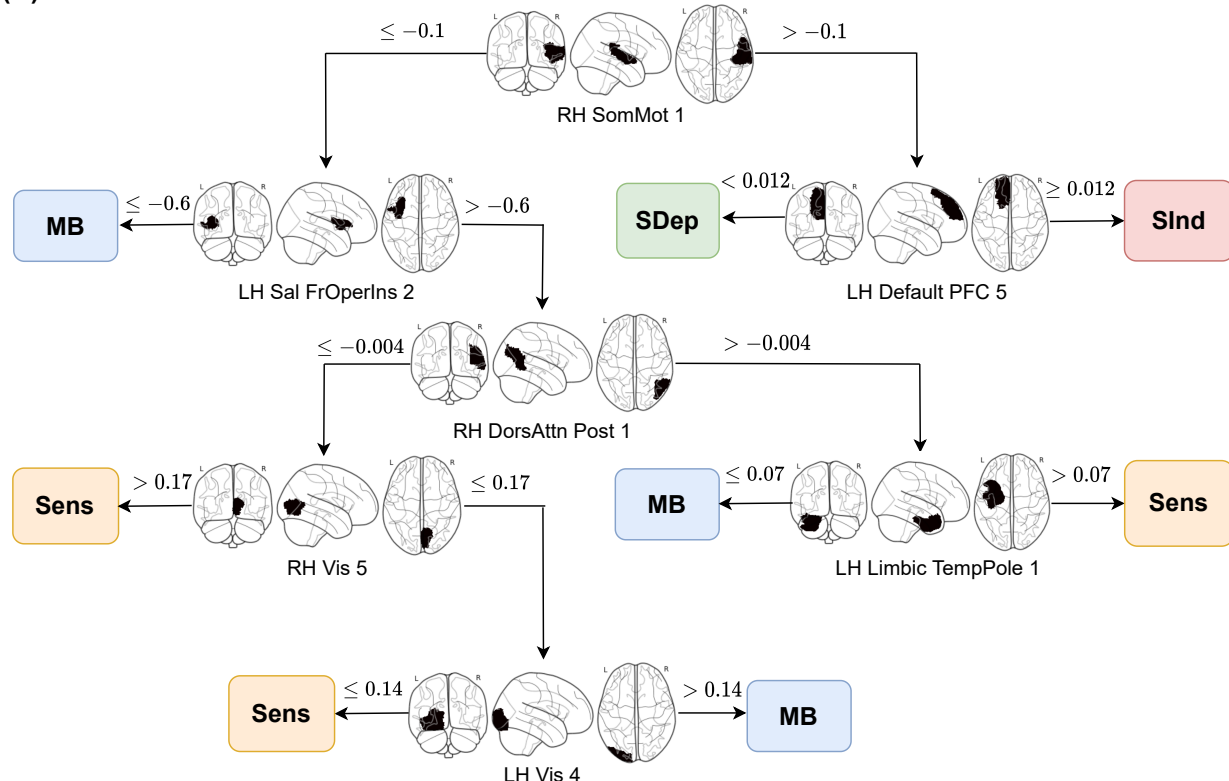


Figure 5. Mind blanking is supported by a segregative brain profile, making it easily classifiable. (A) Diffusion map analysis showed a large range in diffusion values for the periods preceding MB reports, leading to two main clusters broadly encompassing the salience network (blue-range cluster), and the DMN (red-range cluster). The identified small area-to-area transition probabilities indicate a less efficient information flow in MB in comparison to content-oriented states. Note: maps indicate averaged diffusion values across subjects, colorbar indicates z score. (B) Using the diffusion maps as feature vectors in a decision tree classification scheme, showed that the salience network (somatomotor and insular cortices) was able to classify MB by separating it from thought-related reports in fewer steps. Notes: the "less than" relational operator indicates higher resemblance of that cluster to the salience network (blue-range values); the "more than" relational operator indicates higher resemblance of that cluster to the DMN (red-range values).

Table 1. Confusion matrix of mental state classification using averaged diffusion maps for each mental state of each subject as feature vectors and C4.5 classifier

		Classified as			
		MB	Sens	SDep	SInd
Reported	MB	21	8	0	2
	Sens	8	25	0	2
	SDep	0	0	32	4
	SInd	1	0	1	34

Table 2. Classifier performance in classification of each mental state. (FP: false positive, ROC: receiver operating characteristic, TP: true positive).

	TP Rate	FP Rate	Precision	ROC Area
MB	0.677	0.084	0.700	0.838
Sens	0.714	0.078	0.758	0.813
SDep	0.889	0.010	0.970	0.947
SInd	0.944	0.078	0.810	0.917